NUMERICAL SIMULATION OF BUBBLY CAVITATING FLOW IN SHOCK WAVE LITHOTRIPSY

Michel Tanguay and **Tim Colonius**
Division of Engineering and Applied Science
California Institute of Technology
Pasadena, CA 91125
E-mail: michel@caltech.edu

Abstract

The bubbly cavitating flow generated by a lithotriptor is computed using an ensemble averaged two-phase flow model. The time-dependent, compressible flow computation is divided into two separate calculations: the refocusing of a spherical pulse by an ellipsoidal reflector, and the evolution of the steepening wave including the cavitating bubble cloud it generates. The first computation is single phase and is done in prolate spheroidal coordinates in order to have the surface of the ellipsoidal reflector aligned with the computation grid. The output of this simulation is then fed to the two-phase cylindrical coordinates domain. Preliminary results and qualitative comparison to experimental observation are presented.

1 Introduction

Extracorporeal shock wave lithotripsy (ESWL) is a medical procedure used to break kidney stones into fragments small enough for natural elimination. The treatment consists of firing a sequence of focused shock waves into the kidney. A drawback of this approach is that the shock waves can damage the surrounding tissue (Coleman & Saunders 1993; Connors et al. 1996; Willis et al. 1999, 2000). Subcapsular hematomas (bleeding inside the kidney) as well as morphological changes in the kidney are typical side effects of ESWL. Moreover, the procedure may leave small stone fragments behind which then can act as nuclei for the generation of new stones. Many aspects of ESWL remain unclear. For example, it is commonly postulated that cavitation induced by the shock wave is responsible for the stone comminution but this remains unproven. The mechanisms responsible for tissue damage are also ambiguous. Both *in vitro* and *in vivo* experiments have been conducted to attempt to correlate tissue damage with lithotriptor parameters (strength of shock wave, number of shocks, frequency of repetition and shock waveform) as well as the presence of cavitation (Sapozhnikov et al. 2001; Lokhandwalla et al. 2001). From the theoretical stand point, hypotheses have been formulated regarding possible damage mechanisms to the cells stemming from the nearby presence of cavitating bubbles (Lokhandwalla & Sturtevant 2001). If the mechanisms for stone comminution and tissue damage can be clarified, it may be possible to tailor the lithotripsy pulse to optimize its potency while minimizing the damage to the patient.

In order to shed light on the results obtained from experimental lithotriptors, a numerical simulation study is currently in progress. The purpose of the computations is to provide a clearer picture of the progression of the shock wave and the evolution of the cloud of cavitation bubbles it generates. Using the code that we developed, we expect to test some of the hypotheses that have been brought forward with regards to the role of cavitation in stone comminution.

As seen from high speed photography of experimental lithotriptor, clouds of bubbles form near the focal point of the ellipsoidal reflector. Previous attempts in numerical modeling of this bubble cloud consisted for the most part in the time integration of the dynamics of a single bubble in an otherwise spatially uniform media (Rayleigh–Plesset or of a similar model). The experimentally measured time history of the pressure

field (*in vitro*) is used as input to the computation (Songlin & P. 1999; Bailey et al. 1999; Cleveland et al. 2000; Howle et al. 1998). These results are then compared to that of passive cavitation detectors (PCD). However, the presence of a solid object near focus (such as a stone) can significantly change the period between bubble collapse as measure by a PCD (Lokhandwalla 2001). On a more general note, cloud cavitation has been shown to play a significant role in the overall dynamics of bubbly mixture (Wang 1999, 1999; Kumar & Brennen 1993).

The purpose of this paper is to report our progress on the numerical modeling of lithotripsy. Using a combination of the bubbly continuum model and a shock capturing scheme we are able to compute the evolution of a spherical pulse, its reflection off an ellipsoidal mirror and the cavitation field generated by the focusing shock wave. Preliminary results and a qualitative comparison to experimental observations are also presented.

2 Modeling

2.1 Physical aspects of lithotripsy

An electrohydraulic (or spark-gap) lithotriptor is depicted schematically in figure 1. An expanding spherical wave is generated by the spark and is redirected by the ellipsoidal reflector. A typical experimental measurement of the pressure trace at the focal point of the reflector is shown as part of figure 4.

As the reflected part of the pulse converges towards the focus, its amplitude becomes large enough that it steepens into a shock wave. As a consequence of the reflection and focusing, a short period of tension in the liquid is generated resulting in cavitation. Bubbles form in a narrow region as seen in the following sequence of snapshots (figure 2) of a cavitation cloud. From these pictures, the bubbles reach a maximum size of the order of 1 mm.

2.2 The continuum model

We consider a continuum bubbly flow model which is based on the work of Zhang & Properetti (1994a), (1994b). The governing equations for the average property of the bubbly mixture are obtained by ensemble averaging over all possible bubble locations and states (ie radius, rate of expansion, amount of non-condensible gas). The equations are then simplified for low void fraction. Within the approximation of the equations used in this work, the model is similar to the one obtained from the analysis of Biesheuvel & van Wijngaarden (1984). Only a brief discussion of some of the important assumptions of the model is presented here.

The derivation of the bubble model assumes that its interior remains thoroughly mixed and of uniform temperature, which is equivalent to the neglect of heat transfer and diffusion of the vapor into the non-condensible gas within the bubble. Furthermore, the model is based on the assumption that the void fraction remains small, consequently *direct* bubble–bubble interactions are ignored. Bubbles influence one another by changing the void fraction of the phase averaged mixture. The local state of the mixture phase is used for the far field condition seen by a bubble. These approximations are valid provided that the mixture remains dilute and length scales associated with the variation in the average mixture remain large compared to the bubble size. As seen from the previous experimental work (Cleveland et al. 2000), bubbles can reach a size which is much larger than the length scale associated with the lithotripsy shock wave. A realistic model should therefore be able to account for this feature. We are currently working to include this effect into the bubble model, however, the model used in this work does not yet account for this effect.

As it can be expected from the intensity of the tensile (negative pressure) part of the lithotripsy shock wave, the bubble field undergoes explosive like expansion followed by violent collapse. Under collapse, diffusion effects can no longer be neglected. In addition, the violence of the collapse is likely to cause bubble fission and consequently to absorb energy and change the quantity of non-condensible gas present in the bubbles. Modeling bubble fission present a challenge for future work. Some preliminary results are presented by Brennen (2001).

In the derivation of the mixture model, ensemble averages of functions of the states of the bubble field are required. At this stage of our work, we have further assumed that the probability distribution of the bubble states is narrowly peaked around the average values. As a consequence, only the averaged states of

the bubble field needs to be computed. However, it can be shown from experimental results that the bubble size does fluctuate from the ensemble averaged value. We are also currently working the implementation of a probabilistic model for the disperse phase.

3 Numerical method

In order to simulate a realistic lithotriptor, the generation of the pulse by the spark and ellipsoidal reflection as well as the cavitation in the focus region are treated. Since we are interested only in the cavitation occurring in the neighborhood of the focus, we have divided the computational domain into two parts: a pure liquid domain using prolate-spheroidal coordinates and a bubbly mixture domain using cylindrical coordinates. Both domains are treated as axisymmetric with respect to the focal axis.

The various boundary conditions for this work are shown in figure 3. The non-reflective boundary condition used here is similar to the one used in Thompson (1987), and Poinsot & Lele (1992). The artificial buffer zone is a combination of a non-reflective boundary condition, mesh stretching and filtering. This approach follows the work of Colonius et al. (1993). The centerline treatment was based on the work of Mohseni & Colonius (2000).

A compact fourth order Pade finite difference scheme was used in the pure liquid domain to provides a high accuracy for the spatial derivatives. However, as the reflected part of the initial spherical pulse steepens as it converges towards the focus, finite difference methods progressively generate high frequency error. To alleviate this problem, we employed a third order finite volume Essentially Non-Oscillatory (ENO) scheme in the cavitation domain. Since the shock wave travels mainly in the x-direction, the ENO scheme was used to calculate the fluxes in that direction only and the compact finite difference was used in the radial direction.

The implementation of the ENO scheme is similar to that of Harten et al. (1987), Shu & Osher (1988), Harten (1989). A notable feature of our implementation is the assumption of constant void fraction for the purpose of calculating the Jacobian of the mixture fluxes. This not only facilitates the implementation of the algorithm but also allows for the implementation of a more sophisticated model for the bubble dynamics (statistical distribution of the bubble state).

An explicit fifth order Runge–Kutta time marching scheme was used in the reflector domain. Because of the stiffness of the bubble dynamics, a Kaps–Rentrop adaptive time marching scheme was required for the cavitation part of the calculation.

Because of space restrictions, only a brief description of our numerical model has been presented here. A more detailed version will be made available in a forthcoming PhD thesis.

4 Results

4.1 Initial condition

For the cavitation domain, the initial bubble number density and initial bubble radius are needed as well as fluid properties. The initial bubble size is too small to be measured directly from experiments. *A priori* estimates must be validated by comparing parameters such as maximum bubble growth and time between bubble collapses to experimental observations. Based on earlier calculations, we estimate the initial bubble radius to be of the order of $1 - 10\mu$m which is in accordance with values used by other investigators. A value of 1μm was used for the calculations presented in this work. The initial bubble number density is comparatively easier to estimate. Based on high speed photography of cavitating bubble cloud in a laboratory lithotriptor, Bailey (1999) estimated a value on the order of 75 bubbles/cm^3. Some preliminary calculations were performed using this value but was found to generate void fractions beyond the capabilities of our model. In view of this limitation a revised value of 7.5 bubbles/cm^3 was used in these preliminary calculations. This value leads to realistic values of the maximum observed bubble radius.

The fluid properties (density, vapor pressure, viscosity, surface tension) required for the calculation were taken to be those of water at standard atmospheric conditions. The Tait equation of state for water was used.

As mentioned above, an initially spherically expanding shockwave is generated at the spark gap. A detailed modeling of the shock generation is beyond the scope of the present work. We rely in part on the

initial pulse used in the works of Christopher (1994), and Averkiou & Cleveland (1999). However, as noted above, the reflector domain is computed using prolate-spheroidal coordinates in order to accurately represent the geometry of the elliptical reflector. Shock capturing in this coordinate system is an additional challenge not yet met. Therefore, in preliminary work we have used a smoother version of the initial waveform. Our working assumption is that it is possible to find a smooth initial pulse for which shocking is delayed until the pulse reaches the cavitation domain (which is fitted with the ENO scheme), but which has essentially the same pressure profile just upstream of the focus. Figure 5 compares the pressure time history for our smoothed initial pulse at 1 cm away from the origin with those from previous studies.

As can be seen in figure 5, the initial condition is a pure positive pressure pulse. Consequently, a non-zero far field velocity profile must be prescribed in order to assure a purely outgoing wave. However, because of the presence of the reflector, it is not possible to have the velocity field extend to infinity, and we truncate the initial condition at the surface of the reflector. Because of this limitation, the prescribed initial wave also has a radially inwardly propagating component. This has the consequence of producing, near the focus, an exaggerated region of negative pressure in addition to the negative pressure produced (correctly) by the edge wave.

4.2 Preliminary results

In order to gauge the effect of cavitation on the propagation of the pulse, the computations were first carried out without the presence of bubbles. Contours of the pressure field are shown in figure 6 at several instants in time. From these results, it is apparent that the largest contribution to the tensile phase of the pressure measured at focus arises from interaction of the direct wave and the edge of the reflector.

Figure 4 shows the comparison between the numerical and experimental pressure traces at the focal point. The differences between the non-cavitating and experimental waveforms can be attributed to the smoothness and width of the initial pulse. Both of these effects have made the focusing region wider and hence of lower intensity but the general features of the lithotripsy pulse are present.

The introduction of the cavitation in the second domain generated significant difference in the focusing of the shock wave as can be seen in figure 6. The presence of the bubble field in front of the reflected wave attenuates its focusing. Consequently, a lower maximum peak pressure is achieved at focus. The cavitation also changes the propagation of the wave coming off the edge of the reflector. Figure 4 shows in greater detail the impact of the cavitation on the pressure time history at the focus. It is possible that the cavitation generated by the exaggerated region of negative pressure (an artificat of the initial condition) defocuses the wave.

Cavitation is concentrated in a band of approximately 20 mm wide band along the path of the shock wave as seen in figure 7. This value is larger than typical experimental values (approximately 12-15 mm). This discrepancy can be attributed to differences in the initial pulse.

Bubbles reached a maximum size of 1.3 mm in our calculations which is comparable to values observed in experiments. The lifetime of the bubbles varies between 250 to 500 μs. This is in accordance with experimental measurements. In the initial phase of the bubble cloud collapse, a collapse front moves from right to left (figure 7) while in its final phase, the cloud collapse in an ellipsoidal fashion.

From figure 7, it is surprising to find the void fraction one order of magnitude smaller in a region 4 mm wide and 30 mm long centered at the focus. At this stage, we are unsure if this is a consequence of our particular choice of initial conditions or is a phenomenon that occurs naturally in lithotripsy. Since this region is shielded by a shroud of cavitating bubbles, it would hard to establish its existence from empirical observations.

Because of the bubble model used in this work, the bubbles grow back to a significant size after the main collapse. This is contrary to what has been previously observed in experiments. This would suggest that additional damping mechanisms become significant during bubble collapse and, more likely, bubble fission is occurring.

Based on our preliminary results, it is clear that an accurate representation of the initial wave generated by the spark gap is important in order to closely match experimental measurements. A steeper pulse will result in a more confined beam than shown here. Furthermore, an improved model of the initial wave will reduce the tensile tail seen behind the shock wave. This will in turn diminish the cavitation, change the propagation of the edge wave and its interaction with the shock wave.

5 Conclusions

In this paper, we have presented our approach and preliminary results of numerical simulation of lithotripsy. Our computations shares many similarities with previous experimental results. Improvements in the initial conditions and mesh convergence studies are still required to validate our results against experimental observation. However, at this stage we are able to notice interesting features within the cloud such as a region of reduced cavitation around the focus.

Acknowledgements

We would like to thank the PPG investigators, particularly Murtuza Lokhandwalla and Mike Bailey for their insightful comments on this work as well as for sharing their experimental data. This paper is dedicated to the memory of Professor Brad Sturtevant, who provided the "spark" for this work as well as a myriad of useful suggestions; we miss him greatly. This work was supported by NIH under grant PO1 DK43881.

References

Averkiou, M. & R. Cleveland (1999). Modeling of an electrohydraulic lithotriptor with the kzk equation. *Journal of the Acoustical Society of America 106*(1), 102–112.

Bailey, M. (1999). Personal communication.

Bailey, M., D. Blackstock, R. Cleveland, & L. Crum (1999). Comparison of electrohydraulic lithotripters with rigid and pressure-release ellipsoidal reflectors. II. cavitation fields. *Journal of the Acoustical Society of America 106*(2), 1149–1160.

Biesheuvel, A. & L. van Wijngaarden (1984). Two-phase flow equations for a dilute dispersion of gas bubbles in liquid. *Journal of Fluid Mechanics 148*, 301–318.

Brennen, C. (2001). Fission of collapsing cavitation bubble. In *CAV2001: Fourth International Symposium on Cavitation*.

Christopher, T. (1994). Modeling the dornier HM3 lithotripter. *Journal of the Acoustical Society of America 96*(5), 3088–3095.

Cleveland, R., S. O.A., M. Bailey, & L. Crum (2000). A dual passibe cavitation detector for localized detection of lithotripsy-induced cavitation *in vitro*. *Journal of the Acoustical Society of America 107*(3), 1745–1758.

Coleman, A. & J. Saunders (1993). A review of the physical properties and biological effects of the high amplitude acoustic fields used in extracorporeal lithotripsy. *Ultrasonics 31*(2), 75–89.

Colonius, T., S. Lele, & P. Moin (1993). Boundary conditions for direct computation of aerodynamic sound generation. *AIAA Journal 31*(9), 1574–1582.

Connors, B., S. Youzhi, A. Evan, V., L. Willis, & J. Lingeman (1996). Morphological changes observed in the renal vasculature immediately following shock-wave lithotripsy. *Journal of the American Society of Nephrology 7*(9), A2418–A2418.

Harten, A. (1989). Eno schemes with subcell resolution. *Journal of Computational Physics 83*, 148–184.

Harten, A., E. B., S. Osher, & S. Chakravarthy (1987). Uniformly high order accurate essentially non-oscillatory schemes III. *Journal of Computational Physics 71*(2), 231–303.

Howle, L., D. Schaeffer, M. Shearer, & P. Zhong (1998). Lithotripsy: the treatment of kidney stones with shock waves. *SIAM review 40*(2), 356–371.

Kumar, S. & C. Brennen (1993). Some nonlinear interactive effects in bubbly cavitating clouds. *Journal of Fluid Mechanics 253*, 565–591.

Lokhandwalla, M. (2001). Personal communication.

Lokhandwalla, M., J. McAteer, J. Williams, Jr., & B. Sturtevant (2001). Mechanical haemolysis in shock wave lithotripsy (SWL): II. in vitro cell lysis due to shear. Submitted to Physics in Medicine and Biology.

Lokhandwalla, M. & B. Sturtevant (2001). Mechanical haemolysis in shock wave lithotripsy (SWL): I. analysis of cell deformation due to SWL flow-fields. *Physics in Medicine and Biology 46*, 1–25.

Mohseni, K. & T. Colonius (2000). Numerical treatment of polar coordinate singularities. *Journal of Computational Physics 157*, 787–795.

Poinsot, T. & S. Lele (1992). Boundary conditions for direct simulations of compressible viscous flows. *Journal of Computational Physics 101*(1), 104–129.

Sapozhnikov, O., V. Khokhlova, M. Bailey, J. Williams, Jr., J. McAteer, R. Cleveland, & L. Crum (2001). Effect of overpressure and pulse repetition frequency on cavitation in shock wave lithotripsy. To appear in Journal of the Acoustical Society of America.

Shu, C. & S. Osher (1988). Efficient implementation of essentially non-oscillatory shock-capturing schemes. *Journal of Computational Physics 77*(2), 439–471.

Songlin, Z. & Z. P. (1999). Shock wave-inertial microbubble interaction: A theoretical study based on the gilmore formulation for bubble dynamics. *Journal of the Acoustical Society of America 106*(5), 3024–3033.

Thompson, K. (1987). Time dependant bounday conditions for hyperbolic systems. *Journal of Computational Physics 68*(1), 1–24.

Wang, Y.-C. (1999). Effects of nuclei size distribution on the dynamics of a spherical cloud of cavitaion bubbles. *Journal of Fluids Engineering 121*, 881–886.

Wang, Y.-C. & C. Brennen (1999). Numerical computation of shock waves in a spherical cloud of cavitation bubbles. *Journal of Fluids Engineering - Transactions of the ASME 121*(4), 872–880.

Willis, L., A. Evan, B. Connors, P. Bloomgren, & J. Lingeman (1999). The impact of high-dose lithotripsy on renal structure and function. *Contemporary Urology*, 45–50.

Willis, L., A. Evan, B. Connors, & J. Lingeman (2000). Sustained impairment of renal hemodynamics after shock wave lithotripsy. *FASEB Journal 14*(4), A658–A658.

Zhang, D. & A. Properetti (1994a). Averaged equations for inviscid disperse two-phase flow. *Journal of Fluid Mechanics 267*, 185–219.

Zhang, D. & A. Properetti (1994b). Ensemble phase-averaged equations for bubbly flow. *Physics of Fluids 6*(9), 2956–2970.

Figures

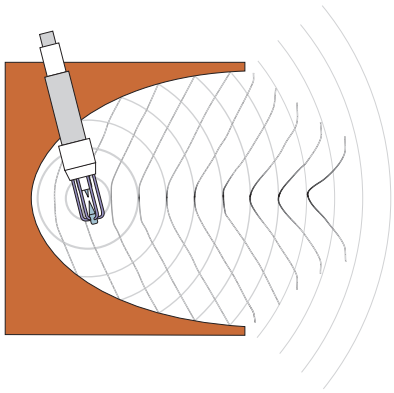

Figure 1: Diagram of reflector and spark generator

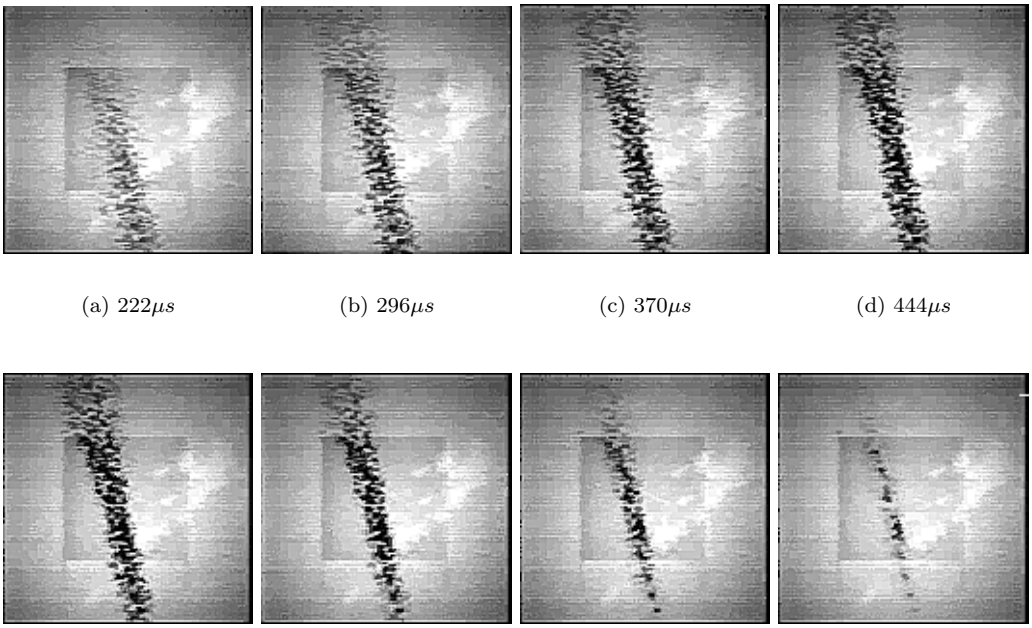

(a) $222\mu s$ (b) $296\mu s$ (c) $370\mu s$ (d) $444\mu s$

(e) $519\mu s$ (f) $593\mu s$ (g) $667\mu s$ (h) $741\mu s$

Figure 2: Snapshots of a bubble cloud near the focus generated by an electrohydraulic lithotriptor. Courtesy of Michael R. Bailey, Center for Industrial and Medical Ultrasound, Applied Physics Lab, University of Washington, Seattle.

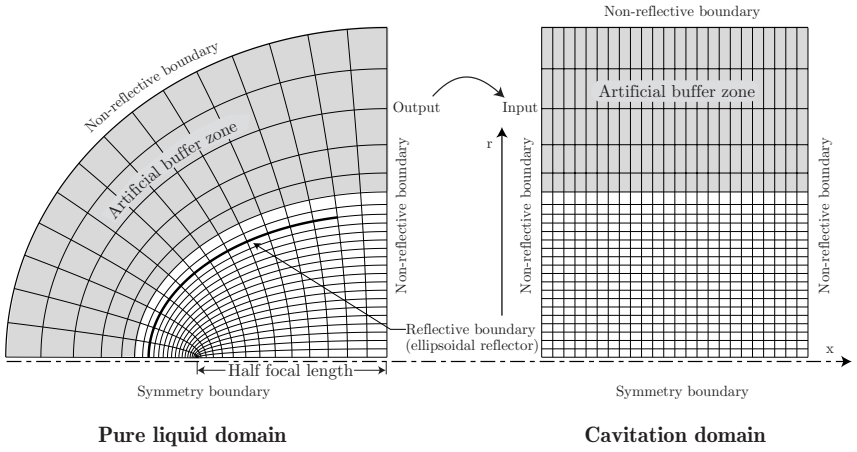

Figure 3: Diagram of the meshes and boundary conditions used for each domain

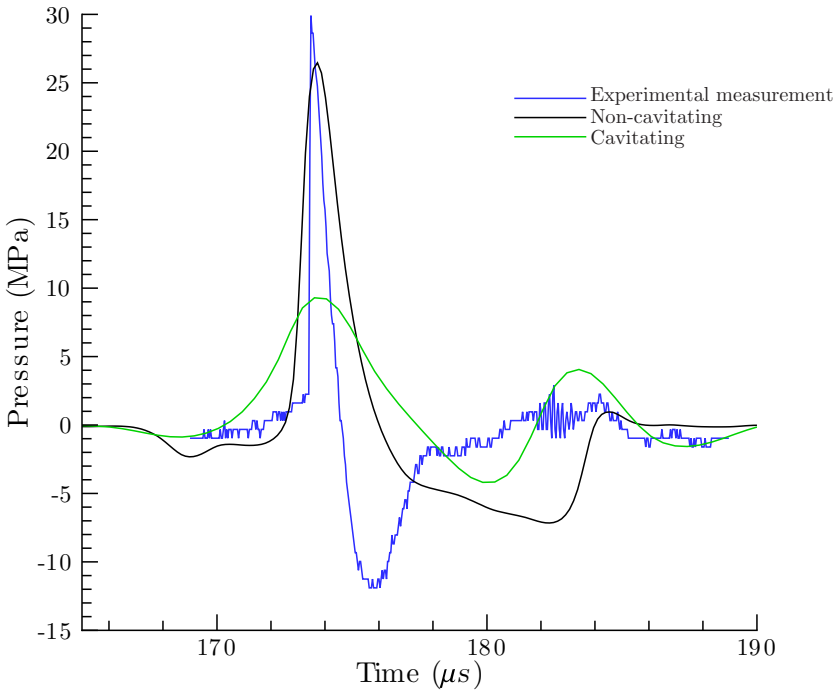

Figure 4: Time history of pressure at focus for cavitating, non-cavitating and experimental results

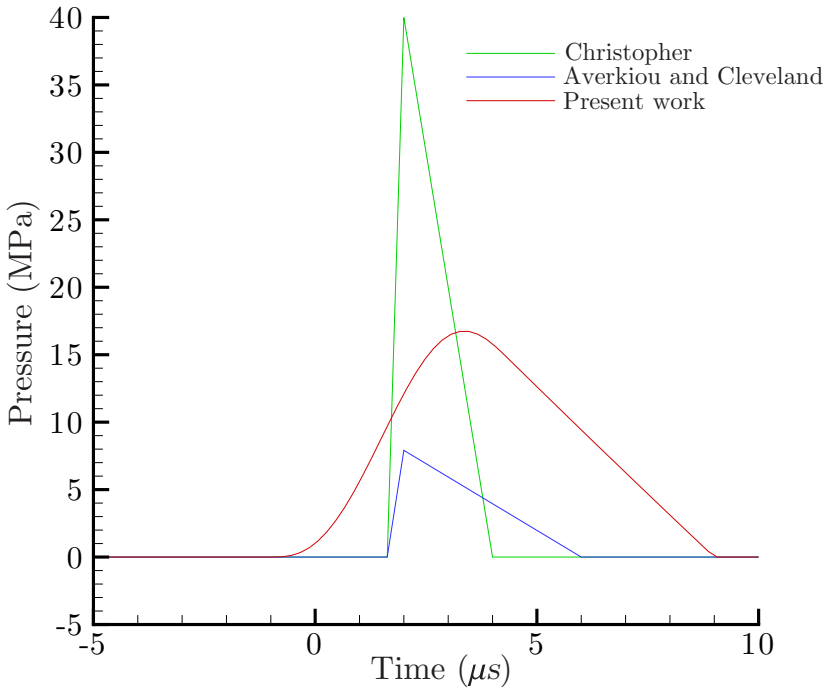

Figure 5: Time history of pressure at 1 cm away from initial focus

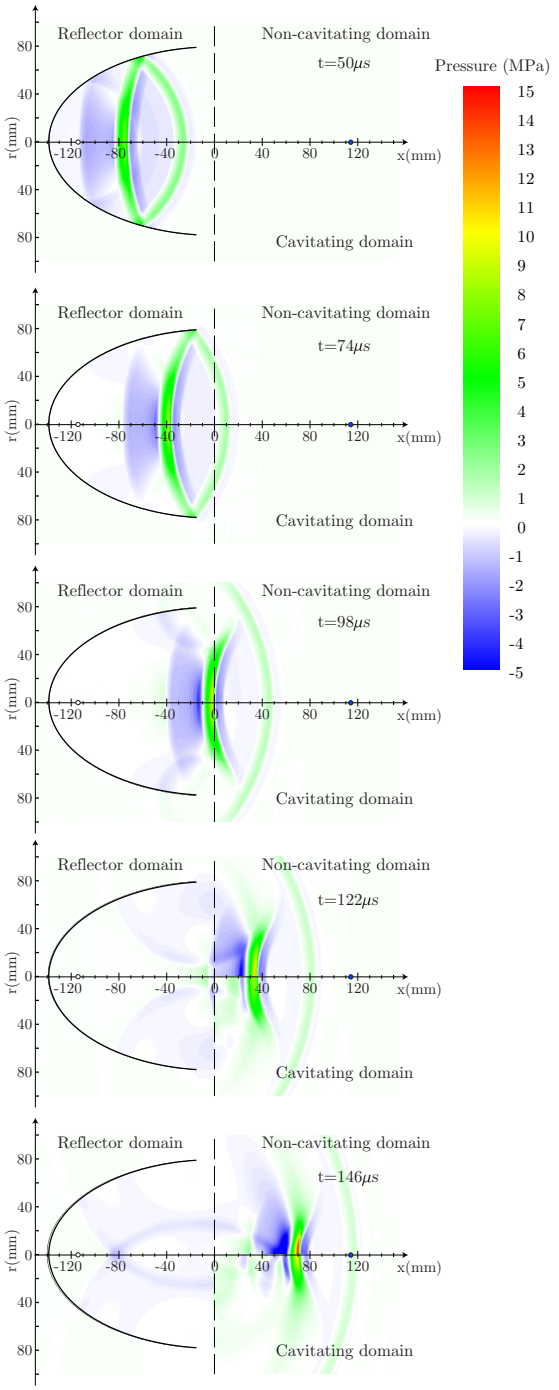

Figure 6: Pressure contour for lithotripsy pulse for both with and without cavitation

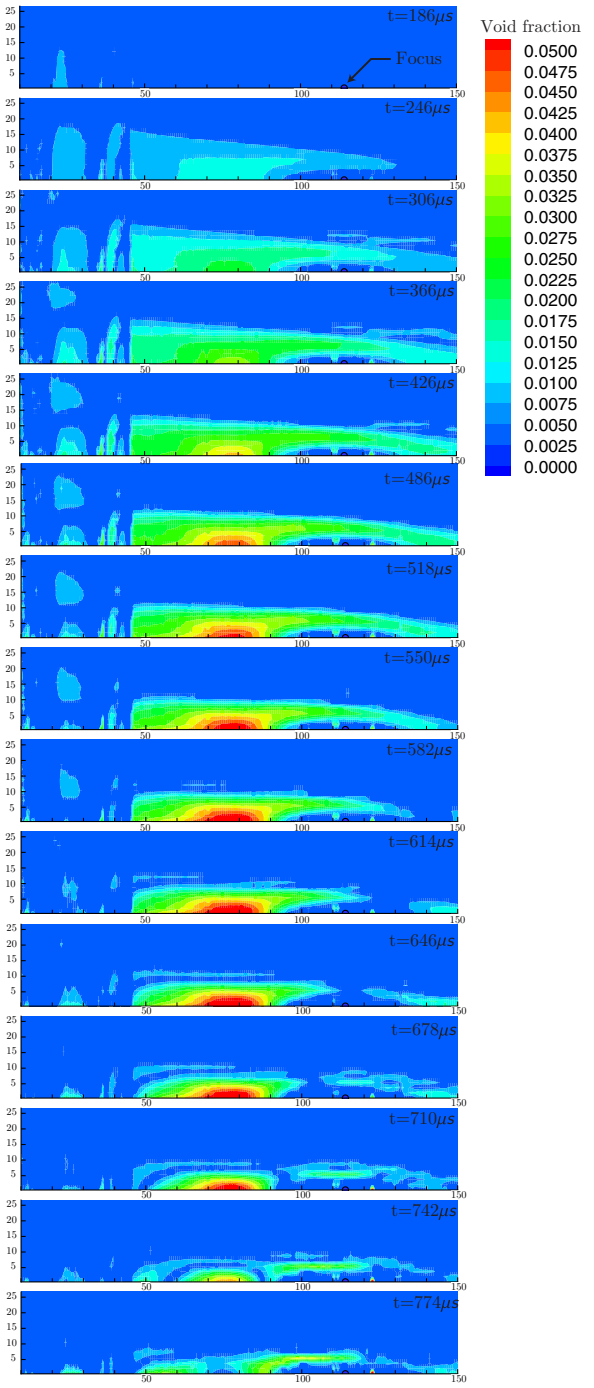

Figure 7: Cavitation cloud: snapshot of the void fraction contour